

Nesprin-2 Giant (NUANCE) maintains nuclear envelope architecture and composition in skin

Yvonne Lüke^{1,*}, Hafida Zaim^{1,*}, Iakowos Karakesisoglou^{1,2,*}, Verena M. Jaeger¹, Lorenz Sellin³, Wenshu Lu¹, Maria Schneider¹, Sascha Neumann^{1,4}, Asa Beijer¹, Martina Munck^{1,4}, V. C. Padmakumar^{1,4}, Joachim Gloy³, Gerd Walz³ and Angelika A. Noegel^{1,4,‡}

¹Center for Biochemistry, Medical Faculty, University of Cologne, Joseph-Stelzmann-Str. 52, 50931 Cologne, Germany

²Department of Biological Sciences, The School of Biological and Biomedical Sciences, The University of Durham, Durham DH1 3LE, UK

³Renal Division, University Hospital Freiburg, 79106 Freiburg, Germany

⁴Center for Molecular Medicine Cologne (CMCC) and Cologne Excellence Cluster on Cellular Stress Responses in Aging-Associated Diseases (CECAD), University of Cologne, Joseph-Stelzmann-Strasse 52, 50931 Cologne, Germany

*These authors contributed equally to this work

‡Author for correspondence (e-mail: Noegel@uni-koeln.de)

Accepted 20 March 2008

Journal of Cell Science 121, 1887-1898 Published by The Company of Biologists 2008

doi:10.1242/jcs.019075

Summary

Giant isoforms, encoded by *Nesprin-1* (*Syne1*) and *Nesprin-2* (*Syne2*), are multifunctional actin-binding and nuclear-envelope-associated proteins belonging to the spectrin superfamily. Here, we investigate the function of Nesprin-2 Giant (NUANCE) in skin by generating mice lacking the actin-binding domain of Nesprin-2 (Nesprin-2 Δ ABD). This loss results in a slight but significant thickening of the epidermis, which is a consequence of the increased epithelial nuclear size. Nonetheless, epidermal proliferation and differentiation appear normal in the knockout epidermis. Surprisingly, Nesprin-2 C-terminal-isoform expression and nuclear envelope localization were affected in certain tissues. Nuclei of primary dermal knockout fibroblasts and keratinocytes were heavily misshapen, displaying a striking similarity to nuclear deformations characteristic of laminopathies. Furthermore, emerin, the protein involved in the X-linked form of Emery-Dreifuss muscular dystrophy (EDMD), was unevenly distributed along

the nuclear envelope in mutant fibroblasts, often forming aggregates in the deformed nuclear envelope areas. Thus, Nesprin-2 is an important scaffold protein implicated in the maintenance of nuclear envelope architecture. Aged knockout fibroblasts readily generated, by alternative splicing and alternative translation initiation, aberrant Nesprin-2 Giant isoforms that lacked an ABD but that were sufficient to restore nuclear shape and emerin localization; this suggests that other regions of Nesprin-2 Giant, potentially including its spectrin repeats, are crucial for these functions.

Supplementary material available online at
<http://jcs.biologists.org/cgi/content/full/121/11/1887/DC1>

Key words: KASH-domain, Mouse knockout, Laminopathies, Nuclear shape, Cell migration, Cell polarity

Introduction

The mammalian nesprins [Nesprin-1 (also known as *Syne1*, *Myne-1* and *Enaptin*), Nesprin-2 (also known as *Syne2*, *Myne-2* and NUANCE) and Nesprin-3] and their single-gene-encoded orthologues (interaptin in *Dictyostelium discoideum*, ANC-1 in *Caenorhabditis elegans* and MSP-300 in *Drosophila melanogaster*) represent a novel class of broadly expressed multifunctional proteins (Starr and Han, 2002; Warren et al., 2005), anchored in the nuclear membrane through their highly conserved C-terminal KASH-domain (Padmakumar et al., 2005; Starr and Fischer, 2005; Tzur et al., 2006).

Nesprin genes generate, through alternative splicing and alternative promoter and/or terminator usage, a multitude of differentially expressed isoforms, differing in domain architecture and length (Warren et al., 2005). The largest Nesprin-1 and Nesprin-2 transcripts predict proteins of 1014 kDa (*Enaptin*) and 796 kDa (NUANCE), respectively (hereafter referred to as Nesprin-1 Giant and Nesprin-2 Giant, respectively) (Padmakumar et al., 2004; Zhen et al., 2002). They are composed of an N-terminal α -actinin-type actin-binding domain (ABD), a massive spectrin-repeat-containing rod segment followed by a KASH domain,

allowing the physical connection of the nucleus to the actin cytoskeleton. By contrast, the much shorter Nesprin-3 lacks an ABD and integrates the nuclear membrane with intermediate filaments through a direct interaction of its N-terminus with plectin (Wilhelmsen et al., 2005). It is thus not surprising that nesprins, and their orthologues in *C. elegans* and *D. melanogaster*, have been implicated in cytoskeleton-dependent processes such as nuclear anchorage and migration (Grady et al., 2005; Starr and Han, 2003; Yu et al., 2006; Zhang, X. et al., 2007). Still, the exact functions of mammalian nesprins remain largely unknown. Recently published results involving Nesprin-1 and Nesprin-2 knockout (KO) mice harbouring KASH-domain deletions indicate crucial roles of these proteins in myonuclear anchorage and motor neuron innervation (Zhang, X. et al., 2007). The multitude of subcellular nesprin localizations and isoform diversity suggests, however, additional functions. Indeed Nesprin-1 and Nesprin-2 isoforms localize at plasma membrane foci, mitochondria, sarcomeric structures, Golgi complexes, the nucleoplasm, and the outer and inner nuclear membrane, where they associate directly with emerin and lamin A/C (Libotte et al., 2005; Mislow et al., 2002a; Mislow et al., 2002b; Warren et al., 2005; Zhang et al., 2005).

Emerin mutations give rise to Emery-Dreifuss muscular dystrophy (EDMD) (Bengtsson and Wilson, 2004), whereas lamin A/C mutations cause various clinically different disorders, collectively called 'laminopathies' (Broers et al., 2006; Burke and Stewart, 2002; Gruenbaum et al., 2005). For their nuclear envelope (NE) localization, Nesprin-1 and Nesprin-2 require an intact lamin A/C network (Libotte et al., 2005; Zhang et al., 2005). Furthermore, in COS7 cells, Nesprin-2 is essential for the NE localization of emerin (Libotte et al., 2005). These particular associations and molecular interdependencies, in conjunction with human diseases linked to other spectrin-repeat proteins, suggest potential roles for nesprins in genetic disorders. Indeed, recently, *Nesprin-1* mutations resulting in the premature termination of the protein were shown to cause recessively inherited cerebellar ataxias in humans (Gros-Louis et al., 2007).

In an effort to better understand the Nesprin-2 biology and explore its potential to cause genetic disorders, we generated the Nesprin-2 Δ ABD mouse, which lacks the ABD of Nesprin-2. Although the mutant mice did not exhibit an overt phenotype, we uncovered novel and essential functions for Nesprin-2 Giant in maintaining epidermal nuclear shape, NE architecture and composition in primary-fibroblast and keratinocyte cell cultures. Considering the multitude of diverse and tissue-specific Nesprin-2 isoforms and the fact that Nesprin-2 Δ ABD knockout mice are partial loss-of-function mutants, our results assert their candidacy in multiple human disorders, including laminopathies.

Results

Generation of Nesprin-2 Δ ABD mice

To generate Nesprin-2 Δ ABD KO mice we deleted three CH1-domain (calponin homology domain 1)-encoding exons (exons 2, 3 and 4), which, together with the CH2 domain, form a functional ABD (Gimona et al., 2002) (Fig. 1A). Positive embryonic stem (ES)-cell clones for homologous recombination were identified by PCR and verified by Southern blot analysis (Fig. 1B,C), and were then used to derive homozygous mice. The Nesprin-2 Δ ABD KO strain was examined over a period of 5 years. Heterozygous and homozygous KO mice did not display any discernible abnormalities and were indistinguishable from their wild-type (WT) littermates. Although a CH1-domain-deficient Nesprin-2 Giant isoform (termed Nesprin-2 Δ ABD) could be detected under some conditions in the KO mice, several lines of evidence discussed here suggest that this mutant is functionally null for Nesprin-2 Giant. Absence of Nesprin-2 Giant in the homozygous mice was verified by western blot analysis of primary-dermal-fibroblast lysates using polyclonal C-terminus-specific anti-Nesprin-2 antibodies (pAbK1) (Fig. 1D,E). Similar to emerin, the C-terminal Nesprin-2 isoforms were still present (Fig. 1D, asterisks) and their expression levels remained unchanged in the KO cells.

For examination of the KO mice, we used monoclonal antibody (mAb) K56-386 directed against the N-terminus of mouse Nesprin-2 Giant (Fig. 1E). Western blot analysis employing K56-386 hybridoma supernatants on proteins immunoprecipitated with pAbK1 from PAM212 [mouse keratinocytes (Yuspa et al., 1980)] cell lysates demonstrated specific detection of mouse Nesprin-2 Giant (Fig. 2A, arrowhead). Affinity purified K56-386 detected an 800-kDa band only in PAM212 and not in HaCaT [human keratinocytes (Boukamp et al., 1988)] cell lysates (Fig. 2B). Thus, K56-386 is a species-specific mAb detecting specifically mouse Nesprin-2 Giant. Immunoblot analysis of COS7 cell lysates expressing various N-terminal Nesprin-2 segments fused to GFP

allowed us to narrow down and identify the reactive epitope to a peptide encoded by exon 9. By generating the Ex9 Δ -GFP fusion, which corresponds to a 22-amino-acid peptide encoded by an exon-9 fragment (Fig. 3A, boxed in red), we could identify the mAb K56-386 epitope (supplementary material Fig. S1 and Fig. 3A).

In PAM212 cells (Fig. 2C-E) and skin sections from newborn WT mice (Fig. 2F) the antibody specifically stained the NE and colocalized with pAbK1-stained structures (data not shown). In skin from KO mice, K56-386 staining was largely absent (Fig. 2G and Fig. 4D); only the use of undiluted primary antibody resulted in an occasional very faint NE staining restricted to some keratinocyte cells (Fig. 2H, arrowhead in inset). A cross-reaction with the paralogue Nesprin-1 Giant molecule was excluded. The staining pattern of Nesprin-1 Giant (Fig. 2I) is clearly distinct from that of Nesprin-2 Giant in WT human (Fig. 2J; mAb K20-478) and mouse (Fig. 2K; mAb K56-386) skin. Whereas Nesprin-1 Giant localized at cell-cell junctions (Fig. 2I, arrows) and weakly at the NE (Fig. 2I, arrowheads), Nesprin-2 Giant staining was restricted to the NE (Fig. 2J,K). The possibility that the faint NE staining is due to a general upregulation of Nesprin-2 as a consequence of a compensation mechanism can be excluded. Silencing of Nesprin-2 Giant unequivocally led to a downregulation of the smaller C-terminal Nesprin-2 isoforms, suggesting a dependency on Nesprin-2 Giant (Fig. 5D).

Presence of differentially expressed C-terminal Nesprin-2 isoforms in Nesprin-2 Δ ABD knockout tissues

Intrigued by the presence of small C-terminal Nesprin-2 isoforms in the knockout fibroblast cells (Fig. 1D), we proceeded with a pAbK1 immunoblot analysis on various WT tissue lysates to gain more insight into their expression profile. Western blots indicated a broad Nesprin-2 expression and revealed multiple tissue-specific isoforms (supplementary material Fig. S2A,B). High levels of expression were detected particularly in the brain, heart and skeletal muscle. A nearly identical expression pattern was observed in skeletal muscle and heart. In these tissues, the antibody detected consistently prominent bands migrating at ~45 and ~95 kDa. In particular, the 45-kDa isoform was highly expressed specifically in heart and skeletal muscle. A major 250-kDa and a minor

Fig. 1. Generation of Nesprin-2-Giant KO mice. (A) Diagram illustrating the partial genomic organization of the *Nesprin-2* (WT) locus coding for the ABD domain (yellow boxes), the targeting construct and the targeted allele (mutant allele). The Nesprin-2-Giant ATG translation start site in exon 1 is indicated with an arrow. The location of the 5' and 3' probes used for Southern blot analysis is also indicated. Primer sets correspond to those used in PCR analysis for identifying the WT (1.2 kb, Primer set 1: 5'-CATAGAACATGCCCTGAC-ATTCCTG-3' and 5'-CTGTTTCTGAGTATTGCATGCGCTTG-3') and mutant (1.1 kb, Primer set 2: 5'-TGTCTGCCTACATGTTACTATGGTC-3' and 5'-TGCGAGGCCAGAGCCACTGTGTAGC-3') alleles. Primers used for RT-PCR are indicated (see Fig. 9 for more details). Ex, exon; E, *EcoRI*; S, *SacI*; K, *KpnI*. (B) Southern blot analysis of mouse-tail DNAs digested with *EcoRI* for 5' analysis and *SacI* for 3' analysis. (C) PCR analysis of DNAs isolated from *Nesprin-2*^{+/+}, *Nesprin-2*^{+/-} and *Nesprin-2*^{-/-} mice. (D) Western blot analysis of HaCaT (human keratinocytes), and primary *Nesprin-2*^{+/+} and *Nesprin-2*^{-/-} (clone 1 and 2) fibroblast homogenates. Blotting with pAbK1 indicates the absence of Nesprin-2 Giant in KO fibroblasts (arrowhead) and the presence of Nesprin-2 C-terminal isoforms (asterisks). For HaCaT cells, ECL signals were obtained after 5-minutes exposure; for dermal fibroblasts, signals were obtained after prolonged detection. (E) Structural features of all known Nesprin-2 isoforms. Major domains are indicated in different colours and shapes. The epitopes and identity of various anti-Nesprin-2 antibodies used are indicated (inverted Y).

~110-kDa Nesprin-2 immunoreactive band was detected in the brain lysate (supplementary material Fig. S2A). Nesprin-2 Giant was detectable as faint bands in the WT tissue lysates only after prolonged enhanced chemiluminescence (ECL) detection. This particular isoform was most prevalent in the brain, skin, kidney and skeletal muscle, as detected by indirect immunofluorescence (data not shown).

Most smaller C-terminal Nesprin-2 isoforms arise presumably from the alternative usage of internal transcription- and/or alternative translation-initiation sites. As anticipated, C-terminal Nesprin-2 isoforms were also present in the respective Nesprin-2 KO tissue lysates. However, even after prolonged ECL exposure, we did not detect Nesprin-2 Giant in these lysates (Fig. 6A, arrowhead). K56-386 immunoblotting further substantiates the absence of Nesprin-

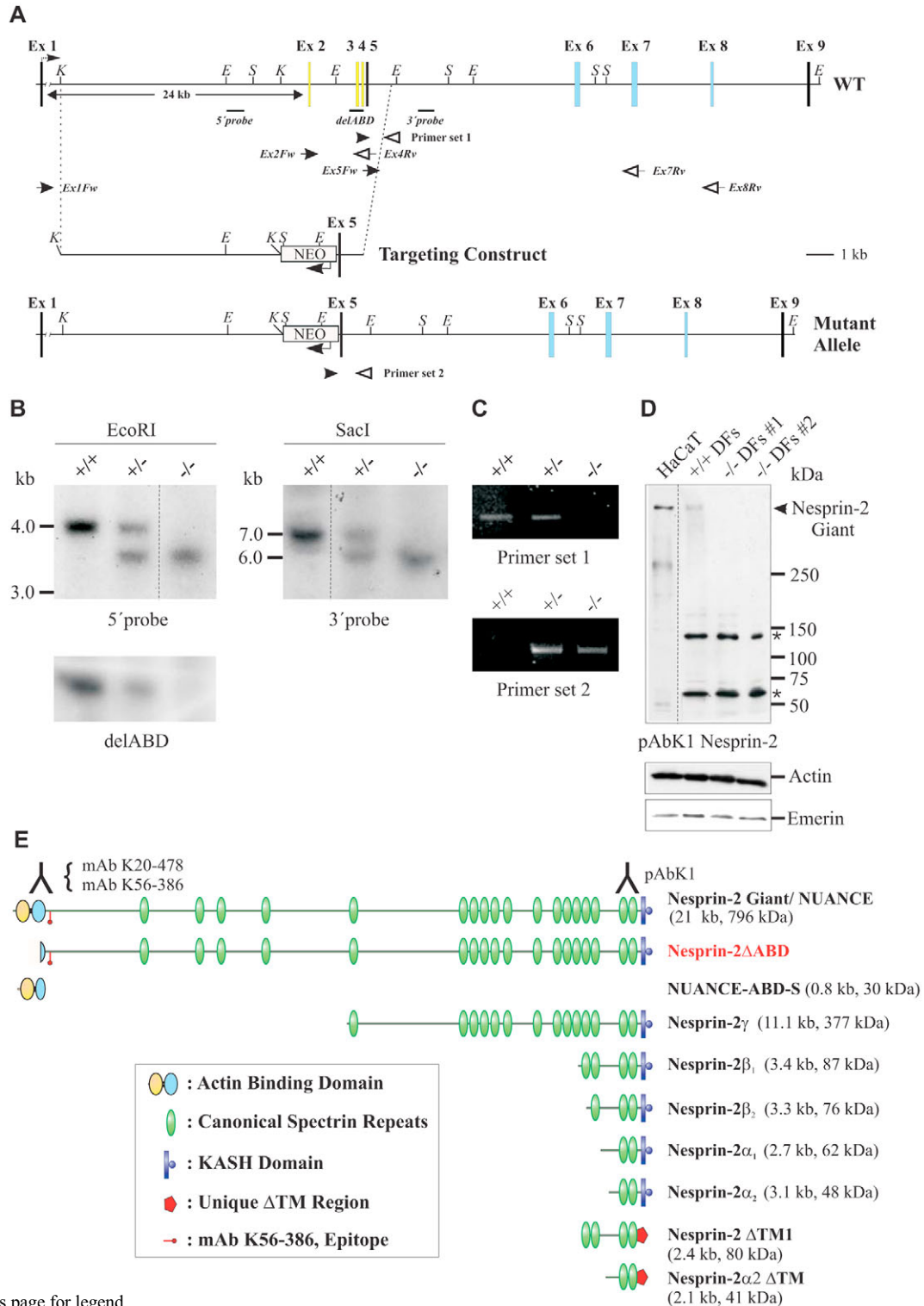


Fig. 1. See previous page for legend.

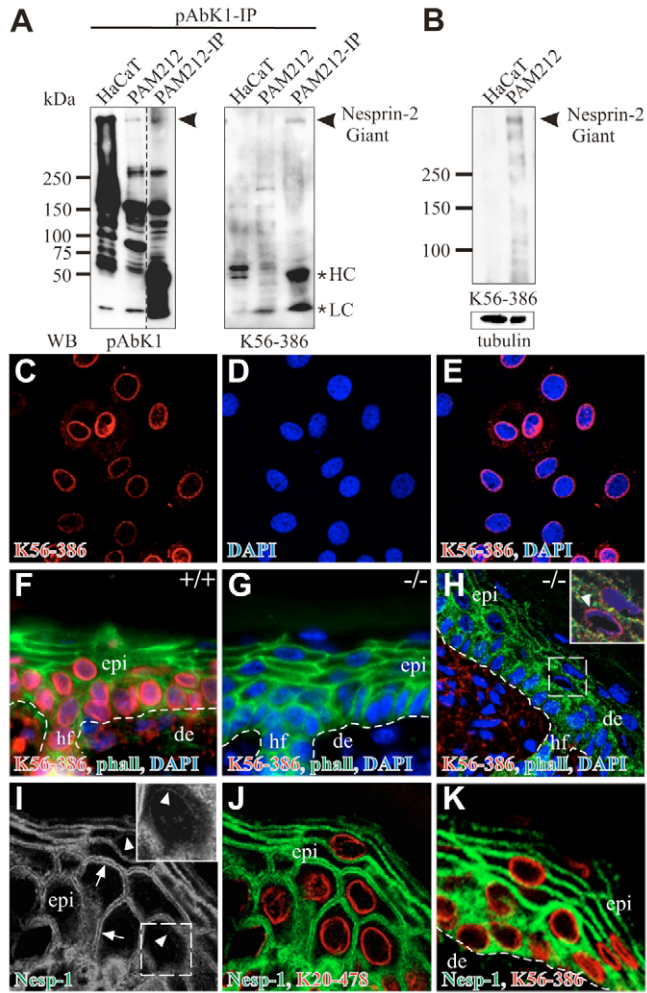


Fig. 2. Characterization of mAb K56-386. (A) Nesprin-2 pAbK1-immunoprecipitated PAM212 samples were probed with K56-386, which specifically recognizes Nesprin-2 Giant (arrowhead). (B) Equal amounts of HaCaT and PAM212 (mouse) cell lysates were probed with K56-386 and anti- β -tubulin (loading control). (C–E) K56-386 (1:10 dilution) stains the NE in PAM212 keratinocytes (C–E) and in WT mouse-skin frozen sections (F), and is largely absent in KO skin (G). (G,H) K56-386 (1:10) staining is largely absent in KO epidermis (G); rarely, some residual NE staining is detectable in isolated regions in the KO epidermis, when K56-386 is used undiluted (inset in H). (I–K) The staining pattern of Nesprin-2 Giant is distinct from that of Nesprin-1 Giant in human (I,J) and mouse (K) epidermis. Nesprin-1-Giant localizes to the NE (I, arrowheads) and to cell-cell junctions (I, arrows). Insets, higher-magnifications of boxed areas. epi, epidermis; de, dermis; hf, hair follicle.

2 Giant in the KO lysates (Fig. 6A). Strikingly, the expression levels and patterns of the Nesprin-2 C-terminal isoforms were affected in the KO tissues (Fig. 6A; summarized in supplementary material Fig. S2B). Only the expression levels of the ~45-kDa and ~95-kDa isoforms in the KO heart and the ~45-kDa isoform in the KO skeletal muscle tissue lysates appeared unaltered when compared with WT samples, whereas, for all other isoforms, we observed either reduced expression levels or their complete absence in the KO tissues. The ~300, ~400, ~600 and 800-kDa, and the ~400 and 800-kDa Nesprin-2 isoforms that were present in WT kidney and skeletal muscle tissue lysates, respectively, were not detectable in the respective KO lysates. Similarly, KO heart tissues expressed

reduced amounts of the ~400-kDa isoform and lacked completely the ~600 and 800-kDa Nesprin-2 proteins. Immunoblotting employing pAbK1 on WT and KO skin lysates revealed significant changes in the expression of the small Nesprin-2 isoforms, whereas Nesprin-2 Giant was undetectable (Fig. 6B).

To get additional insights into the localizations of the Nesprin-2 C-terminal isoform, we examined WT and KO tissues, which differed drastically in their pAbK1 immunoblot pattern of such tissues as skeletal muscle and skin. Immunohistochemical analysis of Nesprin-2 KO skeletal muscle tissue sections revealed an identical staining pattern to WT using pAbK1. In both instances, Nesprin-2 staining was found at the NE (Fig. 6C,D, arrowheads; also see inset) and, in agreement with a previous report (Zhang et al., 2005), also at sarcomeric structures (Fig. 6C,D, arrows).

In summary, our data indicate that Nesprin-2 CH1 exon deletions resulted in a partial knockout of the gene, leading to Nesprin-2 Δ ABD mice, which basically lack the Nesprin-2 Giant isoform and display an altered expression pattern for specific Nesprin-2 C-terminal isoforms in certain tissues.

Nesprin-2-Giant-dependent NE localization of Nesprin-2 C-terminal isoforms

Based on the low expression levels of the Nesprin-2 C-terminal isoform in skin compared with muscle and brain (Fig. 6B), we focused our studies on this tissue. Foremost, Nesprin-2 Giant is highly expressed in skin, and epidermal nuclear positioning is crucial to establish epidermal stratification (Lechler and Fuchs, 2005). In addition, epidermal cornification is accompanied by drastic nuclear morphology changes, resulting finally in dead enucleated squames. It should be noted here that all knockout skin samples employed in the current study were subjected to serial sectioning and sections were first assessed for Nesprin-2 Giant absence (K56-386 negative staining) before the adjacent section was used for further analysis.

Immunohistochemical analysis of WT newborn skin indicated the presence of Nesprin-2 Giant at the NE, at which its staining overlapped with that of pAbK1 (Fig. 4C), which, in addition, weakly stained cytoplasmic structures (Fig. 4B). K56-386 staining was largely absent in KO skin, whereas pAbK1 primarily labelled the cytoplasm. Contrary to WT epidermis, in which a profound NE–Nesprin-2 association was detected with pAbK1 (Fig. 4B, arrowheads in inset), this antibody consistently weakly stained the NE in KO skin (Fig. 4E, arrowhead in inset). This finding contradicts the localization pattern of the C-terminal Nesprin-2 isoforms in KO skeletal muscle tissues, which appeared unaffected by the absence of Nesprin-2 Giant, proposing important roles for Nesprin-2 Giant in the NE-targeting of the smaller C-terminal isoforms in the skin. Moreover, this observation is intriguing considering that the nesprin KASH domain is thought to be sufficient for proper NE targeting (Padmakumar et al., 2005). We assume that the presence of Nesprin-2 Giant further stabilizes and restricts C-terminal nesprin variants at the NE in skin through additional direct or indirect intermolecular interactions. To test this hypothesis, we immunoprecipitated Nesprin-2 Giant from mouse PAM212 keratinocytes using the mAb K56-386. Concomitant western blot analysis with pAbK1 and K56-386 indicated the presence of Nesprin-2 C-terminal isoforms (Fig. 4G, arrowheads) and the Nesprin-2 Giant isoform (Fig. 4G, arrows) only in the Nesprin-2 Giant immunoprecipitated complexes and not in the control samples. It thus appears that Nesprin-2 isoforms form an interconnected network at the NE. Yeast two-hybrid assays using a Nesprin-2 Giant C-terminal segment (aa 6146–6799; last four spectrin repeats) excluded a self-interaction within this part of

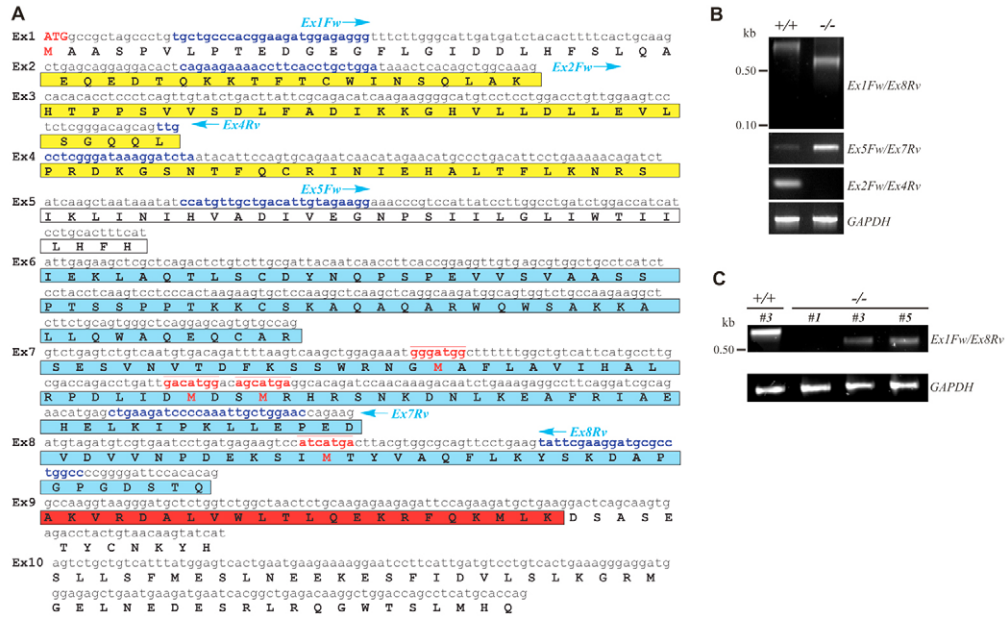


Fig. 3. Generation of the Nesprin-2ΔABD isoform in KO cells and tissues through alternative translational initiation. (A) The coding nucleotide sequences of *Nesprin-2* exons 1-10 are shown and the deduced amino acid sequence is indicated beneath. Similar to other canonical CH1-CH2-type ABDs, the ABD of Nesprin-2 Giant is also encoded by seven exons (CH1-encoded protein sequence is coloured in yellow, linker region in white and CH2 in blue). Exons 2-4 (yellow) were deleted in Nesprin-2ΔABD KO mice. The names and sequences of primers employed in the RT-PCR analysis are indicated in blue lettering. The K56-386 epitope in exon 9 is marked as a red box. (B) RT-PCR analysis of KO- and WT-fibroblast cDNAs using the primer sets indicated in A shows absence of the exon-2-exon-4 region (Ex2Fw/Ex4Rv set). RT-PCR employing exon-1- and exon-8-specific primers (Ex1Fw/Ex8Rv set) on WT- and KO-fibroblast RNA samples did not reveal the anticipated 130-bp exon-1&8 cDNA; instead, a 628-bp KO band was evident, compared with the expected 860-bp WT band (exons 1 through 8). Concomitant sequencing of the KO fragment indicated a splicing event of exon 1 with exon 5. The presence of these exons in the Nesprin-2ΔABD transcript was verified by RT-PCR using the Ex5Fw/Ex7Rv set of primers. Because this alternative splicing event does not result in an open reading frame on the translated transcript, we searched the following exons for alternative initiation sites. Using the Chang Bioscience software (<http://www.changbioscience.com/primo/ti.html>), alternative KOZAK initiation-site sequences were identified in exons 7 and 8 [indicated in boldface (red) and overline in A]. (C) Semi-quantitative RT-PCR analysis of fibroblast cDNAs using the exon-1- and exon-8-specific primer set to show accumulation of the Nesprin-2ΔABD transcript only in aged KO fibroblasts. WT analysis shows the expected 860-bp band (exon 1 through 8), whereas the KO displays the 628-bp band in fibroblasts of higher passages, indicating the alternative splicing event of exon 1 with exon 5. The number of passages is shown (#1, #3, #5).

the molecule (data not shown), therefore suggesting either intermolecular interactions with other Nesprin-2 domains and/or the presence of indirect interactions requiring additional factors.

Nesprin-2 Giant affects the thickness of the epidermal layer and the nuclear morphology in the epidermis

An immunohistological examination (Fig. 7) of the KO epidermis did not reveal gross abnormalities except for an ~25-μm increase ($P=2.6 \times 10^{-33}$, Student's *t*-test) in interfollicular epidermal thickness in the KO (121±17 μm) compared with WT (96±16 μm). Basement membrane appearance and the morphologically distinct stages of keratinocyte differentiation appeared unaltered in KO skin (Fig. 7A,B). Consistent with the well-established staining pattern for integrins in the epidermis, β1 integrin localized in a similar fashion at the perimeter of WT and KO basal cells (Fig. 7C,D). To gain further insights into epidermal-thickness perturbations in KO mice, we assessed proliferation by Ki67 labelling. Mitotic indexes were similar to WT (data not shown) and Ki67 staining was restricted to basal cells (Fig. 7E,F). Counterstaining with phalloidin detected pronounced F-actin ring structures around the NE in KO basal cells (Fig. 7F, arrowhead in inset), similar to WT (not shown), indicating the existence of alternative molecular mechanisms, besides Nesprin-2 Giant, that connect the NE to the actin cytoskeleton. Immunolocalization studies on WT and KO skin sections by using anti-keratin-14 (anti-K14), -K1 and -K10 (Fig. 7G-L) as well as

anti-involucrin and anti-fillagrin antibodies (data not shown) did not reveal any abnormal staining patterns. The mutually exclusive expression pattern of K14 and K1 and/or K10, and the expression of late differentiation markers was maintained in the KO epidermis, suggesting that epidermal differentiation is spatially and temporally maintained.

Consistent with previous data showing that Nesprin-2 Giant is required for the NE localization of emerin in COS7 cells, we observed changes in the emerin localization pattern in the skin (Fig. 8A-F). On the basis of stainings using two different anti-emerin antibodies, we found that, whereas, in the KO epidermis, the emerin pattern at the NE was unperturbed, major alterations were evident in the KO dermis. In WT tissue, the emerin staining was confined to the NE, making dermal-cell identification possible (Fig. 8A-C, arrowheads). In KO tissue, this was no longer possible because of the irregular emerin subcellular staining pattern (Fig. 8F, arrows). However, immunoblotting employing anti-emerin antibodies on several KO and WT skin lysates indicated identical expression levels (data not shown). In summary, the main alteration appears to be an emerin mislocalization specifically in the KO dermis but not in the epidermis, in which emerin localization is unperturbed.

More importantly, the emerin staining revealed an unusual round shape of nuclei, especially for the nuclei of basal KO keratinocytes (inset Fig. 8D). In fact, KO basal as well as suprabasal keratinocyte

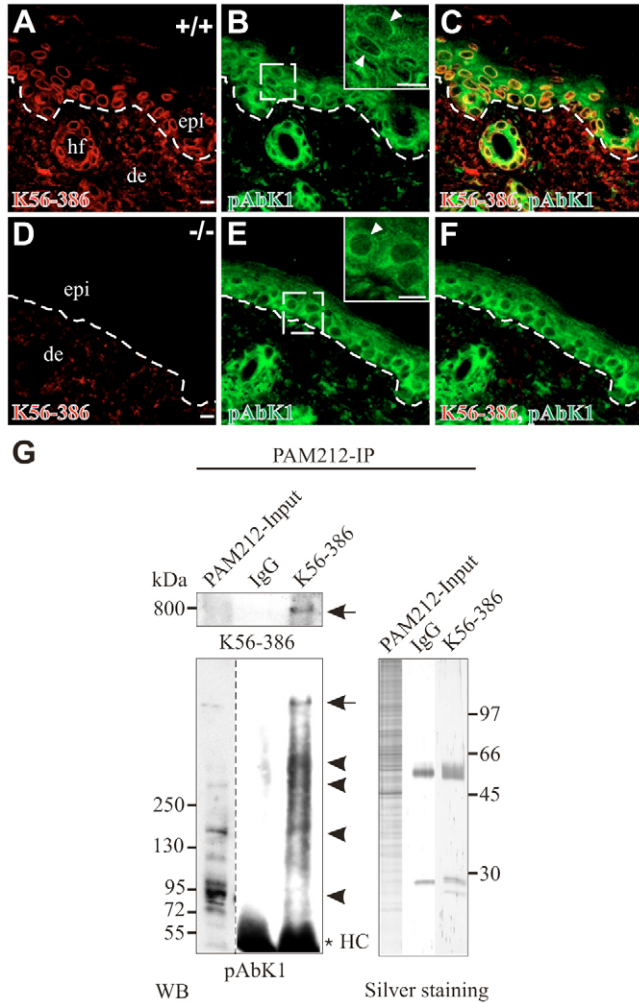


Fig. 4. Localization of the Nesprin-2 C-terminal isoform is affected in KO epidermis. (A-F) WT (A-C) and KO (D-F) frozen skin sections were stained with the N- and C-terminally directed anti-Nesprin-2 antibodies K56-386 and pAbK1. pAbK1 stains the NE in WT (B, arrowheads in inset), which is rarely apparent in the KO epidermis (E, arrowhead in inset). Hf, hair follicle; de, dermis; epi, epidermis. The broken line delineates the location of the basement membrane. Scale bars: 10 μ m. (G) Nesprin-2-Giant-K56-386 immunocomplexes from mouse keratinocytes (PAM212) were probed (WB) with pAbK1 and K56-386. Arrowheads, small C-terminal Nesprin-2 isoforms; arrows, Nesprin-2-Giant isoform. Detection of the 800-kDa band in the K56-386 immunoblot is rarely possible in the input, but clearly visible in the immunoprecipitation lane. For the pAbK1 immunoblot, the sample was run in parallel on a separate gel. Silver staining is used as control (HC: IgG heavy chain).

nuclei appeared much larger when compared to WT (compare Fig. 8C with 8F).

To further examine these changes, primary keratinocyte and fibroblast cells from both WT as well as KO tissues were investigated. Immunolocalization studies with KO keratinocytes indicated heterogeneous K56-386 antibody staining and nuclear morphology variabilities among the cell population. Whereas about 80% of cells (200 counted) lacked any staining, a subset of KO cells (20%) seemed to have undergone a phenotypic reversion, as indicated by the weakly positive and discontinuous staining of K56-386 (Fig. 8G, asterisks) and normal nuclear shape. In the following text, KO cells that were assessed as being K56-386-positive will be referred to as Nesprin-2 Δ ABD cells (Fig. 1E), and K56-386-

Table 1. Nuclear morphology of WT, Nesprin-2-Giant-deficient- and Nesprin-2 Δ ABD-expressing fibroblasts

	Area (μ m ²)	Perimeter (μ m)	Contour ratio
WT	104.4 \pm 4.1	38.5 \pm 1.5	0.85 \pm 0.03
Nesprin-2-Giant deficient	205.7 \pm 9.1	61.2 \pm 2.7	0.69 \pm 0.03
<i>P</i> value	7.15 \times 10 ⁻⁸³	9.2 \times 10 ⁻¹¹⁸	2.96 \times 10 ⁻⁹⁸
Nesprin-2 Δ ABD	175.2 \pm 8.6	50.5 \pm 2.5	0.83 \pm 0.04
<i>P</i> value	9.45 \times 10 ⁻⁴¹	1.75 \times 10 ⁻⁴⁹	3.9 \times 10 ⁻⁷

Nuclear morphometric-parameter analysis of WT and mutant cells. Mean \pm s.e.m. results and the corresponding *P* values (control versus mutant) are indicated. Measurements were performed in triplicate experiments and more than 500 cells were counted for each cell type.

negative cells as Nesprin-2-Giant-deficient. Interestingly, Nesprin-2 Δ ABD-expressing cells exhibited a confined pAbK1 pattern at the NE (Fig. 8H, arrowhead) and a normal nuclear morphology (Table 1). Occasionally, the pAbK1 staining persisted at the NE in Nesprin-2-Giant-deficient cells (Fig. 8H, large arrow). In the majority of Nesprin-2-Giant-deficient cells, however, pAbK1 staining was either redistributed to the cytoplasm or very faint (Fig. 8H, arrows). Cells exhibiting such a localization of the Nesprin-2 C-terminal isoform showed a remarkable nuclear morphology (53.2%; 200 counted). These nuclei were highly lobulated (Fig. 8I, inset), exhibiting irregular nuclear shapes and profound nuclear blebbing (Fig. 8I, arrows). In WT primary keratinocyte cells, anti-Nesprin-2-Giant and pAbK1 antibodies strongly stained the NE, and nuclei had a normal morphology (Fig. 8J-L). The extent of nuclear lobulations in KO cells as compared with WT was determined by calculating their respective nuclear contour ratios ($4\pi \times \text{area}/\text{perimeter}^2$; >500 counted for each cell type). The contour ratio for a circle is 1, and this number decreases in misshapen nuclei (Goldman et al., 2004). Whereas WT cells exhibited a contour ratio of 0.85, this value significantly decreased to 0.69 in Nesprin-2-Giant-deficient cells. These changes reflect a 1.97-fold increase in the mid-plane cross-sectional area and a 1.58-fold increase in the perimeter length in KO nuclei (Table 1).

Whereas Nesprin-2 Δ ABD cells displayed similar contour ratios to WT cells, their mean area and perimeter values were significantly larger than those of WT (Table 1), indicating important roles for the CH1 domain in the maintenance of nuclear size. In summary, our data suggest that Nesprin-2 controls nuclear morphology and nuclear size in keratinocytes.

Silencing of Nesprin-2 Giant in human keratinocytes affects nuclear shape and the Nesprin-2 C-terminal isoform pattern

To further substantiate the functions of Nesprin-2 Giant, we designed shRNAs against the CH2 domain and analyzed their effects on the NE in HaCaT cells. Immunofluorescence analysis employing a Nesprin-2-Giant-specific antibody (K20-478) indicated a loss of Nesprin-2 Giant in 10% of the transfected cells. Silencing of Nesprin-2 Giant caused an unmistakable nuclear phenotype, in contrast to cells transfected with control RNAi plasmids (Fig. 5A). Loss of Nesprin-2 Giant resulted in variable NE morphological changes, from minor NE blebbing to severely misshapen and giant nuclei (Fig. 5A,C, arrows). The percentage of cells displaying NE defects was clearly increased in Nesprin-2-Giant-silenced cells when compared with controls (Fig. 5B). Furthermore, contour-ratio values dropped from 0.87 in control cells to 0.73 in Nesprin-2-Giant-silenced cells (Table 2). Loss of Nesprin-2 Giant also affected the Nesprin-2 C-terminal isoforms (Fig. 5C). In cells exhibiting

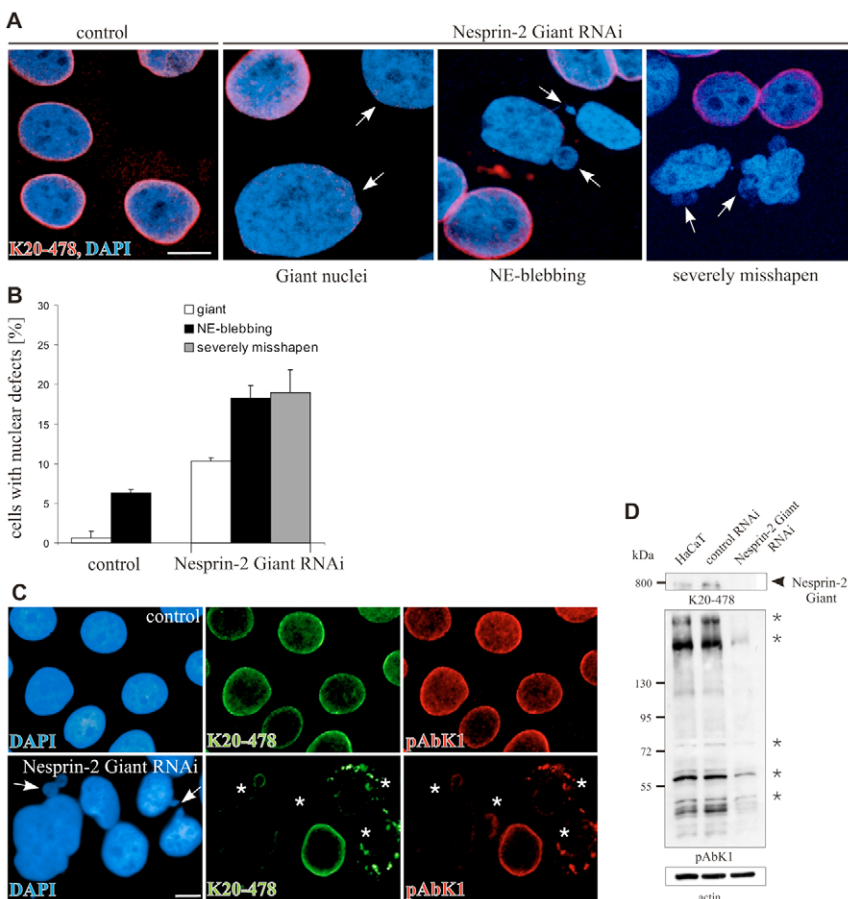


Fig. 5. Silencing of Nesprin-2 Giant in human keratinocytes affects nuclear shape and Nesprin-2 C-terminal-isoform localization. (A) Indirect immunofluorescence analysis of control and Nesprin-2-Giant-silenced HaCaT cells using Nesprin-2-Giant-specific antibodies (K20-478) and Nesprin-2 polyclonal (pAbK1) antibodies; the latter also detects the C-terminal isoforms. Note that the pAbK1 pattern is affected or absent in Nesprin-2-Giant-silenced cells (asterisks). Nuclei are stained by DAPI. Scale bar: 10 μ m. Confocal images are shown. (D) Immunoblot analysis of Nesprin-2-Giant-silenced human keratinocytes and control cells. Note the loss of the 800-kDa Giant isoform (arrowhead) in Nesprin-2-Giant-silenced human keratinocytes. Silencing of the Nesprin-2-Giant isoform also results in a downregulation of the smaller isoforms (*) detected by pAbK1. Actin is shown for control.

Nesprin-2-Giant silencing, pAbK1 staining was either weak or colocalized with abnormal aggregates of Nesprin-2 Giant (Fig. 5C, asterisks). Downregulation of the Nesprin-2 C-terminal isoforms could also be verified by immunoblot data (Fig. 5D), thus indicating a dependency on Nesprin-2 Giant of the smaller isoforms.

Roles of Nesprin-2 Giant in NE architecture and NE composition in fibroblasts

We next examined primary KO dermal fibroblasts by indirect immunofluorescence staining with K56-386 (detects Nesprin-2 Giant and Nesprin-2 Δ ABD) or pAbK1 (detects all isoforms). Both antibodies gave similar results, except that pAbK1 gave higher cytoplasmic signals, as expected. We found that, in contrast to WT cells (Fig. 9A), K56-386 staining in early-passage mutant cells was largely absent (Fig. 9C) and was accompanied by massive nuclear deformations (Fig. 9D, arrowheads). Similar to KO keratinocytes, and in contrast to WT fibroblasts, in which pAbK1 detected clearly the NE (Fig. 9E, arrows), pAbK1 detected

cytoplasmic structures in a subpopulation of mutant cells and did not reveal a nuclear rim pattern (Fig. 9G, arrows). This abnormal localization was accompanied by nuclear defects (Fig. 9H, arrowheads). Strikingly, mutant cells showing a clear pAbK1 NE

Table 2. Nuclear morphometric-parameter analysis of WT and Nesprin-2-Giant-silenced cells

	Area (μ m ²)	Perimeter (μ m)	Contour ratio
WT	170.4 \pm 9.8	49.3 \pm 2.9	0.87 \pm 0.05
Nesprin-2 Giant RNAi	191.9 \pm 11.1	57.5 \pm 3.3	0.73 \pm 0.04
<i>P</i> value	2.03 \times 10 ⁻⁷	1.6 \times 10 ⁻¹²¹	3.34 \times 10 ⁻⁴⁷

Mean \pm s.e.m. results and the corresponding *P* values (control versus mutant) are indicated. Measurements were performed in duplicate experiments and 300 cells were counted for each cell type.

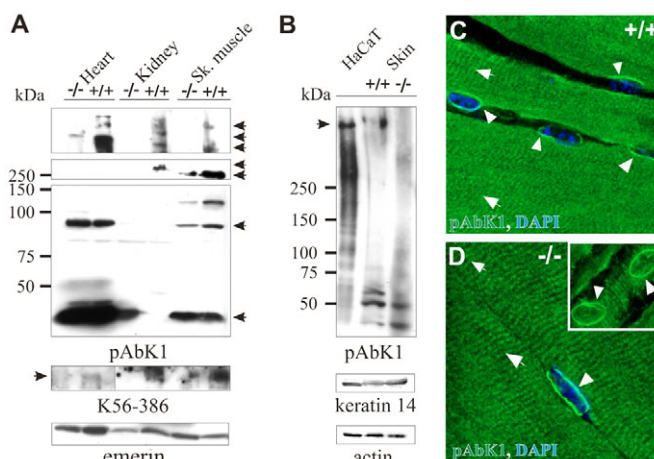


Fig. 6. Nesprin-2-Giant KO mice are partial loss-of-function mutants. (A,B) pAbK1 immunoblot analysis of various WT and KO tissue homogenates (equal amounts loaded). Certain pAbK1-reactive Nesprin-2 C-terminal isoforms are present (arrows) and their levels are perturbed in specific KO tissues. Nesprin-2 Giant is absent in KO lysates. K56-386 detects Nesprin-2 Giant only in the WT (A). Emerin staining shows minor changes. (C,D) pAbK1 detected sarcomeric structures (arrows) and the NE (arrowheads) in WT (C) and KO (D) adult-mouse skeletal muscle frozen sections. DAPI, nuclei.

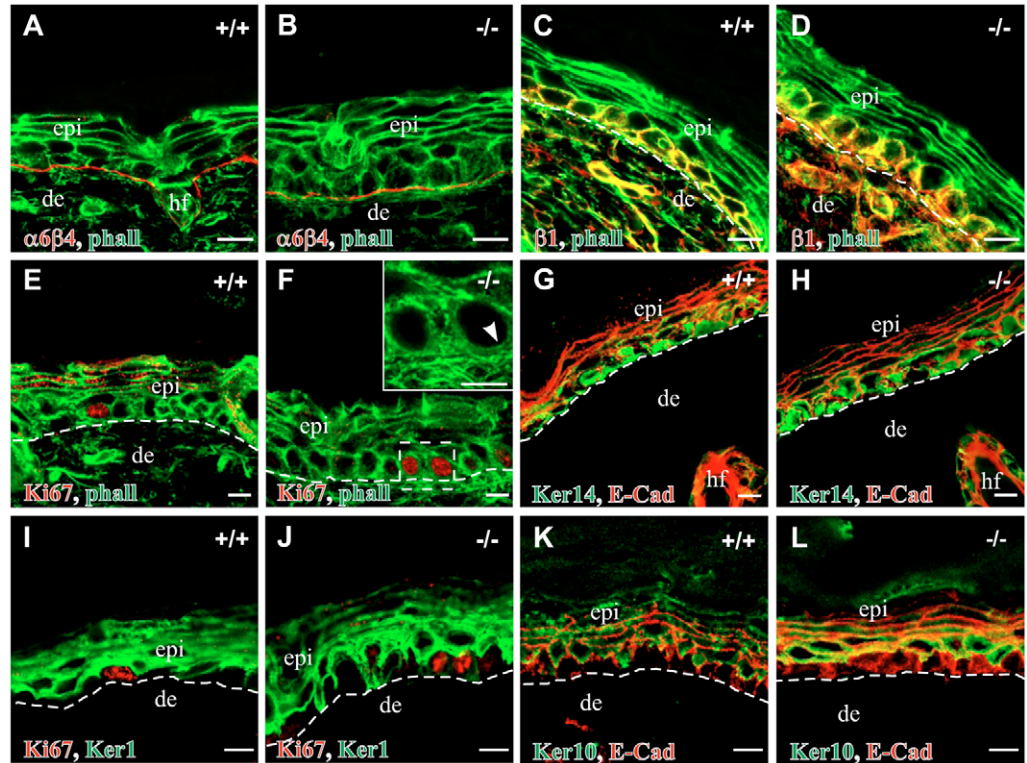


Fig. 7. Epidermal proliferation and differentiation appears normal in KO epidermis. Skins from day-4 WT (A,C,E,G,I,K) and KO (B,D,F,H,J,L) mice were fixed, sectioned and stained with antibodies and with phalloidin to label F-actin. Colour codings correspond to the secondary antibodies or phalloidin used in each case. Note the increased KO epidermal thickness. Inset, higher-magnification of the boxed area. $\alpha 6\beta 4$, $\alpha 6\beta 4$ integrin; $\beta 1$, $\beta 1$ integrin; phall, phalloidin; Ker14, Keratin 14; Ker1, Keratin 1; Ker10, Keratin 10; E-Cad, E-cadherin; epi, epidermis; de, dermis; hf, hair follicle. Scale bars: 10 μ m.

localization (Fig. 9G, asterisk) did not show an overt nuclear phenotype (Fig. 9H, asterisk). Collectively, the mutant fibroblast nuclei were irregular in shape, occasionally exhibiting minor or major NE blebs and lobulations (Fig. 9I-L, arrowheads). Surprisingly, the abnormal nuclear phenotype was restricted only to early-passage (<4) cells. Whereas, at passage 3, approximately 20% of mutant nuclei were abnormal, this number decreased in aged cultures (passages >6) to 4%, which was comparable to WT fibroblasts (Fig. 9O). An immunofluorescence examination of the mutants with anti-Nesprin-2-Giant antibodies indicated that this rescue effect coincided with the presence of K56-386 staining at the NE (Fig. 9M) and with the presence of Nesprin-2 Δ ABD isoforms in the aged fibroblast cultures (supplementary material Fig. S3).

Primary KO fibroblasts also exhibited abnormal emerin localization. Emerin appeared unevenly distributed along the NE and profoundly accumulated in the deformed nuclear areas (Fig. 9Q-S). Whereas lamin A/C levels were unaltered in KO cells (data not shown), their localization was perturbed in mutant cells. Lamin A/C formed abnormal honeycomb structures preferentially in the deformed NE areas in mutants (supplementary material Fig. S4). Altogether, our data suggest important functions for Nesprin-2 in nuclear architecture and composition.

However, the residual K56-386 staining in KO skin (Fig. 2H) and in the established KO cell cultures was still puzzling. One possibility, which we intensively investigated and which still cannot be excluded, was the alternative use of unknown exons located upstream of the deleted ABD exons. However, extensive searches of the mouse EST databases indicated that the sole usage of exon 1 was for the translational initiation site in the Nesprin-2-Giant transcript (Fig. 3A). We then examined whether abnormal splicing events involving exon 1 and downstream exons caused the generation of a novel Nesprin-2-Giant transcript (Nesprin-2 Δ ABD)

lacking exons 2-4. In particular, alternative splicing between exons 1 and 8 would yield a protein harbouring the K56-386 epitope (Table 3). Reverse transcriptase (RT)-PCR employing exon-1- and exon-8-specific primers on WT and KO fibroblast RNA samples did not reveal the anticipated 130-bp exon 1&8 cDNA; instead, a 628-bp band appeared for KO samples, compared with the expected 860-bp WT band that was observed (exons 1 through 8) (Fig. 3B). Sequencing of the 628-bp fragment indicated an abnormal splicing event of exon 1 with exon 5. Because this fusion does not result in an open reading frame on the translated transcript, we searched the following exons for alternative initiation sites. Indeed, we found three Kozak consensus sequences within exon 7 and one within exon 8 (marked and overlined in red, Fig. 3A). In summary, our data favour alternative translation-initiation usage, resulting in a 'semi-functional' Nesprin-2-Giant protein lacking a section, encompassing most of the ABD, of more than 215 N-terminal amino

Table 3. Partial exon-intron organization of Nesprin-2 Giant

Exon	5' codon	3' codon	Exon size (bp)	Intron size (bp)
1	1	1	79	24,186
2	2	3	62	1717
3	1	3	96	110
4	1	3	78	88
5	1	3	93	7576
6	1	2	188	1884
7	3	1	197	2660
8	2	3	101	3419
9	1	3	102	2447
10	1	3	138	4921

The nucleotide position (1, 2 or 3) of the codon triplets at the 5' and 3' ends in the individual exons (1-10) is indicated. Note that only alternative splicing involving exons 1 and 8 would ensure synthesis of a K56-386-reactive Nesprin-2 Δ ABD isoform in the KO mice. Exon and intron sizes are shown.

acids (Nesprin-2 Δ ABD; Fig. 1E); however, this protein is still sufficient to rescue the nuclear abnormalities of Nesprin-2 KO cells.

Nesprin-2 affects fibroblast migration

On the basis of the well-documented role of nesprin orthologues in lower eukaryotes in nuclear positioning and migration, and recent evidence that nuclear repositioning is an initial polarizing event in migrating fibroblasts (Gomes et al., 2005), we investigated the migratory response of primary Nesprin-2-Giant KO and WT fibroblasts after scratch wounding. We used three independent WT and five different KO primary fibroblast cells to perform the wounding assays. A 700- μ m-wide wound was introduced on the cell monolayers and their migrational properties were monitored over time. Whereas WT ($n=3$) cells closed the wound after 20 hours, exhibiting a mean 40 ± 4.9 μ m/hour migration speed, KO ($n=5$) cells

migrated much slower, at 29 ± 1.2 μ m/hour, leaving the scratched wound practically unclosed (Fig. 10). The results were statistically significant ($P=0.03$; Student's t -test), indicating a requirement for Nesprin-2 in the migration of dermal fibroblasts. To examine in more detail the mutant cell phenotype, we submitted wounded WT and Nesprin-2-Giant monolayers 6 hours after the introduction of the scratch to an immunofluorescence analysis and stained for γ -tubulin and the Golgi complex, which are well-known structures that reorient when cells polarize. In $76\pm 2.6\%$ and $84\pm 6.8\%$ of WT cells, repositioning of the Golgi (Fig. 10I,I') and MTOC (Fig. 10J,J'), respectively, takes place within a 120° area facing the wound. By striking contrast, only $34.2\pm 3.7\%$ and $39.0\pm 3.8\%$ of mutant cells exhibited a polarized Golgi complex (Fig. 10I,I') and MTOC (Fig. 10J,J'), respectively. In summary, our data suggest novel roles for Nesprin-2 in cell migration and cell polarity.

Discussion

We demonstrate here novel structural functions for Nesprin-2 Giant in nuclear morphology and architecture in the skin. These functions were further corroborated by *in vitro* cell-culture studies, including Nesprin-2 silencing. Indeed, $\sim 20\%$ of primary dermal fibroblasts and $\sim 53\%$ of primary KO keratinocytes harboured severely misshapen nuclei. The pronounced severity of nuclear morphology abnormalities in keratinocytes suggests profound roles of Nesprin-2 Giant in this particular cell type, which is in accordance with the rather high expression levels of Nesprin-2 Giant in the epidermis as compared with the dermis. As cells aged in culture, these defects diminished, resulting finally in WT-like cells at later passages because of the expression of an abnormally spliced Nesprin-2 Δ ABD transcript, which was confirmed by immunoblotting. Nesprin-2-Giant-deficient fibroblasts display reduced growth rates when compared with WT cells (data not shown). Our data indicate that expression of Nesprin-2 Δ ABD rescues major defects of the mutant cells, allowing them most probably to propagate faster and to finally overgrow Nesprin-2-Giant-deficient cells.

To explain the generation of Nesprin-2 Δ ABD, we favour the usage of alternative translational start sites, which might lead to a deletion of at least 215 amino acids from the N-terminus of Nesprin-2 Giant. Even though the exact starting site remains to be identified, this abnormal protein would lack the CH1 (exons 2-5) domain, the linker region (exon 6) and at least 30 amino acids of the CH2 domain. The absence of the major F-actin-binding sites of the ABD (Winder et al., 1995) in combination with observations that single CH domains are not sufficient to mediate F-actin binding (Gimona and Winder, 1998) suggests that Nesprin-2 Δ ABD might not bind to actin filaments. Although this still warrants experimental validation, such thoughts imply that Nesprin-2-mediated actin association is not required for the structural integrity of the nucleus, but that rather this might be secured by the presence of the massive spectrin-repeat-containing rod (Bennett, 1990).

Surprisingly, the observed KO fibroblast and keratinocyte defects did not result in apparent abnormalities in skin morphology and histology of KO animals. We discovered a mildly thickened epidermis, which we believe is related to the increased keratinocyte nuclear size. Thus, these data confirm both *in vivo* as well as *in vitro* that Nesprin-2 Giant affects nuclear morphology. In fact, a recent report implicates Nesprin-2 Giant in progeria and proposes a structural reinforcer role at the NE (Kandert et al., 2007).

Nuclear-size increase has been associated with nuclear lamina CxxM motif proteins such as lamins and kugelkern (Brandt et al., 2006; Prufert et al., 2004). Therefore, our results suggest that lamin-

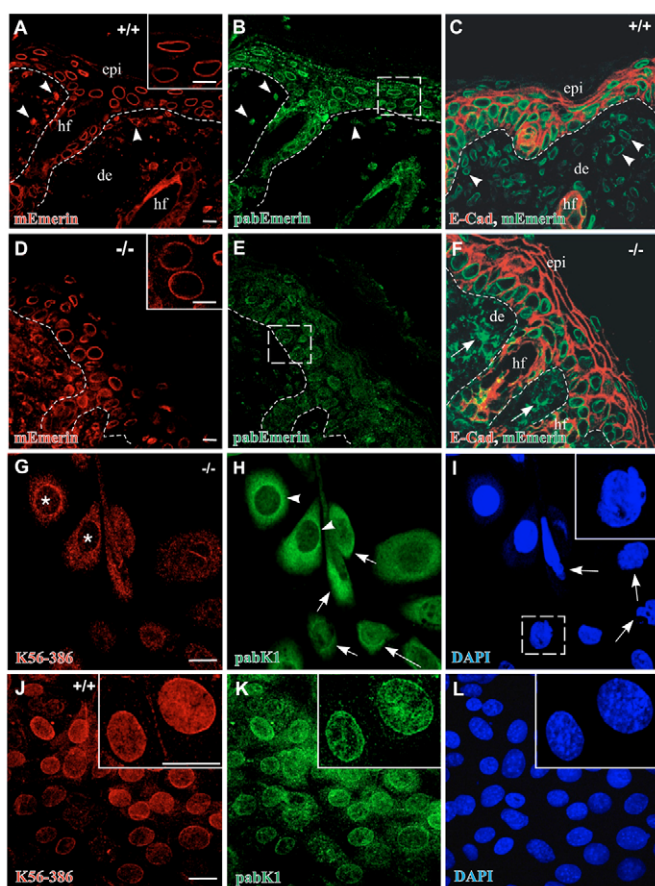


Fig. 8. Nesprin-2 Giant affects nuclear morphology and size in the epidermis. (A-F) WT (A-C) and KO (D-F) frozen skin sections were stained with emerin-specific antibodies as indicated in the lower left of each frame. Note the increased nuclear size of KO epithelial cells. Emerin staining is NE-restricted in WT dermal cells (arrowheads, A-C), whereas, in the KO dermis (D,E and arrows in F), an abnormal staining pattern is evident. (G-L) Primary KO (G-I) and WT (J-L) keratinocytes were subjected to indirect immunofluorescence using anti-Nesprin-2 antibodies as indicated. K56-386-negative cells have an abnormal pAbK1 staining and misshapen nuclei (arrows, H,I). Cells exhibiting weak K56-386 staining (asterisks, G) have a normal nucleus and have pAbK1 staining at the NE (arrowheads, H). Note that the K56-386 and pAbK1 stainings are restricted to the NE in WT cells (K). Insets in J-L are higher-magnifications from another area of the same cover slip. Insets in A,D,I are higher-magnifications of the respective boxed areas in B,E,I, respectively. Confocal images are shown. epi, epidermis; de, dermis; hf, hair follicle. Scale bars: 10 μ m.

related effects on nuclear volume are partially nesprin mediated, because nesprins depend on an intact lamin A/C network for proper NE localization (Libotte et al., 2005; Zhang et al., 2005).

However, epidermal proliferation and differentiation appeared unaltered in the KO epidermis. Recent evidence suggests that transition from a single-layered ectoderm in the mouse embryo to a stratified functional epidermis is triggered by asymmetric cell divisions (Lechler and Fuchs, 2005). However, it remains uncertain whether these events are functionally coupled with nuclear movements, similarly to the actin-based rearward nuclear repositioning to establish MTOC polarization in migrating fibroblasts (Gomes et al., 2005), or, if so, whether alternative and not mutually exclusive microtubule-dependent nuclear-positioning mechanisms exist in the epidermis. Irrespectively, our data suggest that Nesprin-2 Giant might not be required for these cellular events in the epidermis. Alternatively, KO skin homeostasis might be established and maintained either by the persistence of the short Nesprin-2 C-terminal KASH-domain-containing isoforms in the KO skin, or the functional overlap with other nesprin proteins, or both. On the basis of the Nesprin-1 localization pattern in skin, it is, however, unlikely that this particular protein accounts for Nesprin-2-function redundancy. Anti-Nesprin-1 antibodies stained profoundly the keratinocyte cell periphery, a finding that has not been described previously, thus suggesting additional roles for this protein besides its well-known functions at the NE.

It is important to note that Nesprin-2-Giant-deficient fibroblasts (only early passages were examined in the current study) exhibited migration and cell polarity defects. Whether these defects are attributed solely to an abnormal nucleokinesis or are in addition combined with major cytoskeletal rearrangements in the mutant fibroblasts warrants further examination. Nesprin-1 associates directly with the kinesin-II subunit KIF3B; together, these proteins facilitate the accumulation of vesicles at the spindle and midbody (Fan and Beck, 2004). On the basis of the overall structural and primary sequence similarity between Nesprin-1 and Nesprin-2, it cannot be excluded that microtubule-associated motor-protein functions are also affected in Nesprin-2 Giant mutant cells.

An important clue that reinforces the scaffolding aspects of Nesprin-2 Giant at the NE is the reported mislocalization of its C-terminal variants and of emerin in fibroblasts. We hypothesize that Nesprin-2 Giant interacts either directly or indirectly with its shorter C-terminal isoforms, and restricts them at the NE. We favour in particular direct intermolecular interactions of the spectrin repeats, considering that the C-terminal spectrin repeats of Nesprin-1 α have been shown to mediate homodimerization (Mislow et al., 2002a). More importantly, if this hypothesis holds true, it suggests that additional molecular

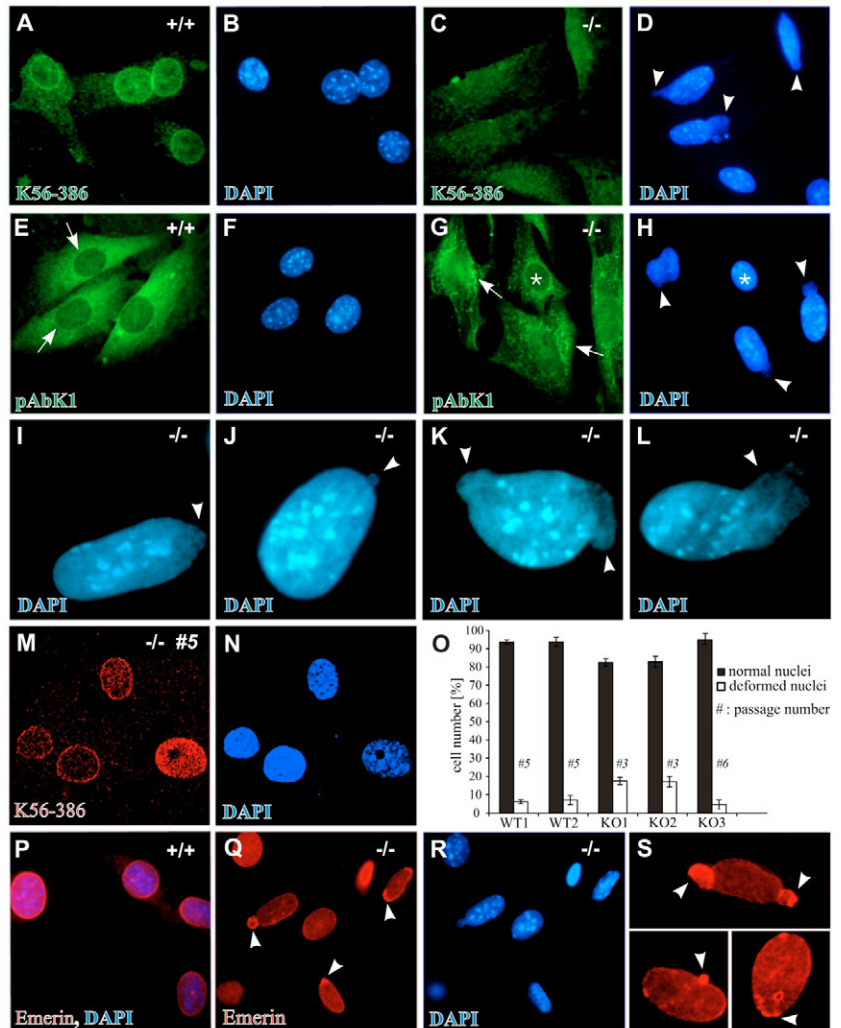


Fig. 9. Nuclear architecture and emerin localization is affected in Nesprin-2-Giant KO fibroblasts. In WT cells (A,B,E,F), Nesprin-2 Giant (A) and C-terminal isoforms (pAbK1; E, arrows) are present at the NE, whereas primary KO cells (C,D,G,H) are negative for Nesprin-2 Giant (C), display strong pAbK1 staining in the cytoplasm (arrows, G) and exhibit severely misshapen nuclei (arrowheads, D,H). Representative nuclear changes are shown in I-L. Note that a pAbK1 NE staining in KO cells coincides with a normal nuclear architecture (asterisks, G,H). (M-O) In higher-passage (>5) KO cells, the mutant nuclear defects diminish (N,O), presumably due to the weak expression of an abnormally spliced Δ CH1Nesprin-2-Giant protein (M). (O) Histogram representing a statistical evaluation of control and mutant cells (percentage of cells; >700 cells counted for each cell type) displaying nuclear deformations. The passage cell number is indicated at the middle of each individual histogram. Error bars denote s.d. Significant *P* value for control versus early-passage mutants = 4×10^{-5} (Student's *t*-test). (P-S) Immunostainings, employing emerin-specific antibodies, of WT (P) and KO (Q-S) cells. In contrast to WT (P), emerin is unevenly localized at misshapen NEs in KO cells (arrowheads, Q). (S) Representative examples are shown in S. Note the emerin accumulation and clustering in the deformed NE regions (arrowheads). Confocal images are shown.

associations besides the well-established interaction between the nesprin KASH-domain and Sun proteins (Padmakumar et al., 2005; Starr and Fischer, 2005; Tzur et al., 2006) in the nuclear lumen might account for a tighter association of the nesprin Giant isoforms with the NE.

The affected emerin NE localization in the KO dermis and fibroblasts is a very important result, considering that the described KO mice exhibit only a partial loss of Nesprin-2 functions. Thus, our findings verify previous emerin-localization studies in COS7

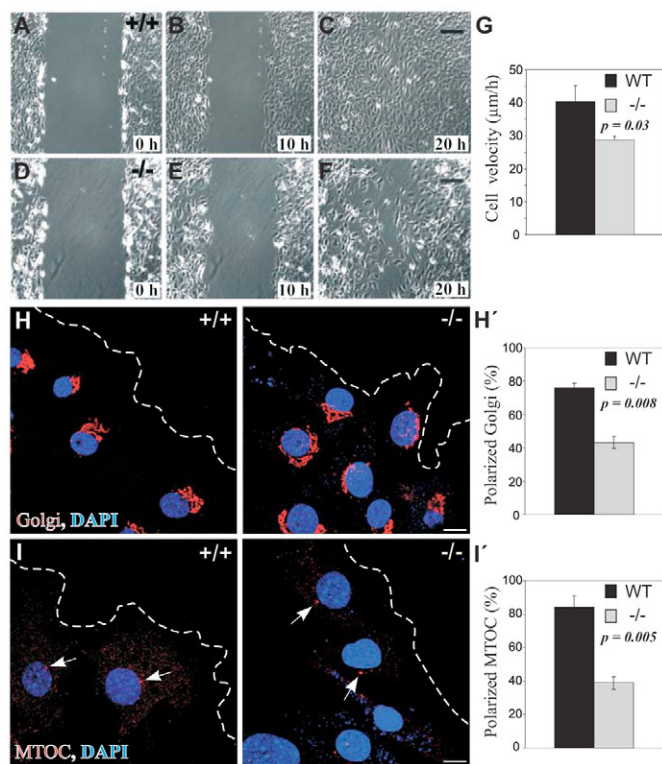


Fig. 10. Loss of Nesprin-2 Giant affects fibroblast migration and cell polarity. (A-F) In contrast to WT fibroblasts (A-C), wounds generated by scratching remain unclosed in Nesprin-2-Giant-deficient fibroblasts (D-F). Fibroblasts of passage 2 were used and KO fibroblasts were verified to be negative for K56-382 staining prior to usage. A representative experiment is shown from three separate experiments. Scale bars: 200 μm . (G) Mutant cells exhibit a statistically significant reduced migration velocity. Mean values and s.d. were calculated from three different primary WT and five different mutant cell cultures, which were assayed in triplicate experiments. (H,I) Indirect immunofluorescence examination of WT and Nesprin-2-Giant-deficient cell monolayers 6-hours post-wounding, using antibodies against Golgi (GM130; row H) and MTOC (γ -tubulin; row I). The broken lines indicate the migrating cell front, which was visualized by FITC-phalloidin counterstaining. Note that both the Golgi complex and MTOC are not positioned towards the wound edge in the mutants. (H',I') Statistical evaluation of the representative experiments shown in H,I indicates a defective cell polarization in Nesprin-2-Giant mutants. Cells with Golgi structures (500 cells counted for each cell type) and MTOCs (300 cells counted for each cell type) positioned within a 120° sector facing the wound edge were assessed as polarized. Error bars denote s.d. from three different experiments. The statistical significance (P values; Student's t -test) is also indicated. Scale bar: 10 μm .

cells, which indicated a requirement for Nesprin-2 Giant. Furthermore, they propose that Nesprin-2 mutations in humans might cause diseases similar to the loss of emerin, which results in EDMD. Finally, the striking similarity of Nesprin-2 KO nuclear abnormalities to laminopathies provides impetus in identifying Nesprin-2 as well as Sun protein mutations in human disorders.

While this paper was under review, Zhang et al. published an article demonstrating that Nesprin-1 and Nesprin-2 heterozygous missense mutations are involved in the pathogenesis of EDMD (Zhang, Q. et al., 2007). The authors also show that Nesprin-1 or Nesprin-2 siRNA knockdown experiments in fibroblasts result in nuclear-morphology changes and affect emerin localization. These data collectively suggest that EDMDs might be caused, in part, by a nucleo-cytoskeleton uncoupling due to disturbances in nesprin-emerin-lamin interactions.

Materials and Methods

Generation of Nesprin-2 Δ ABD mice

KO mice were generated by InGenious Targeting Laboratory (<http://www.genetargeting.com>). The gene-targeting vector is composed of a 9.0-kb *KpnI* mouse 129/Sv genomic fragment upstream of exon 2 (5'-arm), the neomycin cassette and a 950-bp (3'-arm) PCR fragment (amplified using the 5'-ATCACACCTGCAGATTCACAGG-3' and 5'-CTTACTCTGTAATCCAGTCTG-3' primers) containing exon 5 and the downstream intronic sequences. The vector was linearized by *NotI* and transfected by electroporation into 129/Sv ES cells. ES cells harbouring the desired targeting event were identified by PCR, confirmed by Southern blot analysis and microinjected into C57/BL6J host blastocysts. Chimeras and their positive progenies were backcrossed with C57/BL6J mice and crossed to obtain KO mice.

Cell culture and wounding assays

Skin tissues from newborn mice were treated overnight with dispase (10 mg/ml) to separate and isolate the dermis and epidermis, which was then trypsinized (5-10 minutes). Dermal fibroblasts were cultured at 37°C, 5% CO₂ in DMEM supplemented with 10% fetal calf serum (FCS), penicillin and streptomycin. To study migration, confluent serum-starved primary fibroblast monolayers were wounded by scraping cells away with a P200 pipette tip, and were examined using a Leica DM IRE2 microscope and software. Keratinocytes were cultured in low-calcium FAD medium (2/3 DMEM + 1/3 Ham's F12) supplemented with Chelex-treated 10% FCS Gold, 0.18 mM adenin, 0.5 $\mu\text{g/ml}$ hydrocortison, 5 $\mu\text{g/ml}$ insulin, 10 ng/ml EGF, 10⁻¹⁰ M cholera toxin, 5 $\mu\text{g/ml}$ glutamin, 0.05 mg/ml vitamin C, penicillin and streptomycin. Cells were grown at 32°C, 5% CO₂ in 100-mm dishes supported with a mitomycin-C-treated 3T3 fibroblast feeder layer.

RNA-interference

Human Nesprin-2-Giant knockdown was accomplished by plasmid-based RNA-interference (RNAi). Oligonucleotides were constructed using RNAi-Central (http://katahdin.cshl.org:9331/RNAi_web/scripts/main2.pl) as follows: Oligo A, 5'-AACCAGAAGATGTGGATGTTGAAGCTTGAACATCCACATCTTCTGGTTTTT-3'; Oligo B, 5'-GATCAAAAAACCAGAAGATGTGGATGTTCAAGCTTCAACATCCACATCTTCTGGTTCG-3'. Oligonucleotides were annealed and cloned into *BseRI* and *BamHI* sites of pSHAG-1 (Paddison et al., 2002).

Antibodies and immunofluorescence microscopy

A DNA fragment encoding an N-terminal Nesprin-2-Giant segment (Nesprin-2-ABDII; XP_922176; aa 224-493) was generated by PCR, using primers 5'-GGATCCGCTCAGGAGCAGTGTGCCAGGTCTGA-3' and 5'-GAATTCTATT-CACAGAGTCTGTGGACTGG-3', and cloned as *BamHI-EcoRI* fragment into pGEX-2T (GE Healthcare). The recombinant protein was purified using GST-Sepharose beads and isolated after overnight thrombin cleavage at 4°C. mAb K56-386 was produced by immunizing mice with the purified Nesprin-2-ABDII protein and ImmunEasy mouse adjuvant as described previously (Schleicher et al., 1984).

Back skins from 4-day-old mice were placed in OCT compound (Sakura), frozen at -80°C and processed for sectioning. Immunofluorescence was performed as described previously (Zhen et al., 2002). Morphometric analysis of the nuclei was computed using the Leica DM FW4000 IRE2 microscope software.

For immunohistochemistry and immunofluorescence, the following antibodies were used: against Nesprin-2, K56-386 (IF, 1:10; WB, undiluted), K20-478 (Zhen et al., 2002) (IF, 1:500; WB, undiluted), pAbK1 (polyclonal antibody; IF, 1:50; WB, 1:500), Nesprin-1 (Padmakumar et al., 2004) (IF, 1:50), GFP, K3-184-2 (WB, 1:10), β -tubulin (mAb WA3, gift from U. Euteneuer, Ludwig-Maximilians-Universität, München, Germany; WB, 1:1000), γ -tubulin (GTU-88, Sigma; IF, 1:200), α 6 β 4 integrin (IF, 1:50; gift of C. Niessen, University of Cologne, Cologne, Germany), β 1 integrin (Chemicon; IF, 1:200), Golgi (GM130, BD Transduction Laboratories; kindly provided by S. Höning, University of Cologne, Cologne, Germany), Ki67 (Dako; IF, 1:50), Keratin 1 and 10 (Covance; IF, 1:500), Keratin 14 (Covance; IF, 1:1000), Involucrin (Covance; IF, 1:1000), mAb emerin (Novocastra; IF, 1:50), pAb emerin (Acris; IF, 1:50) and E-cadherin (Zymed; IF, 1:50). Secondary antibodies for indirect immunofluorescence analysis were conjugated with Cy3 (Sigma), FITC (Sigma), Alexa Fluor 488 (Molecular Probes, Leiden, NL) and Cy5 (Chemicon). Nuclei were stained with 4, 6-diamino-2-phenylindone (DAPI) and F-actin with FITC or TRITC-conjugated phalloidin (Sigma).

Immunoblotting and immunoprecipitation

Tissues were dissected out, submerged in liquid nitrogen and crushed in a mortar. Crushed tissue and cells were lysed in RIPA buffer. Samples were centrifuged at 14,000 g at 4°C for 30 minutes; the supernatants were mixed with the protein sample buffer and processed through a syringe, and assessed by SDS-PAGE and concomitant Coomassie Blue staining. Proteins were separated on 3-15% gradient SDS-PA gels and blotted overnight at 30 V by tank transfer onto a PVDF membrane (Millipore; blotting buffer: 25 mM Tris/HCl pH 8.0, 186 mM Glycin, 0.1% SDS, 10% ethanol). Membranes were incubated with the corresponding antibodies and immunoreactive bands were revealed by ECL (enhanced chemiluminescence). Nesprin-2 immunoprecipitations were performed as described previously (Libotte et al., 2005).

We thank C. Niessen for reagents and helpful discussions and S. Yuspa for Pam212 cells. This work was supported by the CMMC and the DFG.

References

- Bengtsson, L. and Wilson, K. L. (2004). Multiple and surprising new functions for emerin, a nuclear membrane protein. *Curr. Opin. Cell Biol.* **16**, 73-79.
- Bennett, V. (1990). Spectrin-based membrane skeleton: a multipotential adaptor between plasma membrane and cytoplasm. *Physiol. Rev.* **70**, 1029-1065.
- Boukamp, P., Petrussevska, R. T., Breitkreutz, D., Hornung, J., Markham, A. and Fusenig, N. E. (1988). Normal keratinization in a spontaneously immortalized aneuploid human keratinocyte cell line. *J. Cell Biol.* **106**, 761-771.
- Brandt, A., Papagiannouli, F., Wagner, N., Wilsch-Brauninger, M., Braun, M., Furlong, E. E., Loserth, S., Wenzl, C., Pilot, F., Vogt, N. et al. (2006). Developmental control of nuclear size and shape by Kugelkern and Kurzkern. *Curr. Biol.* **16**, 543-552.
- Broers, J. L., Ramaekers, F. C., Bonne, G., Yaou, R. B. and Hutchison, C. J. (2006). Nuclear lamins: laminopathies and their role in premature ageing. *Physiol. Rev.* **86**, 967-1008.
- Burke, B. and Stewart, C. L. (2002). Life at the edge: the nuclear envelope and human disease. *Nat. Rev. Mol. Cell Biol.* **3**, 575-585.
- Fan, J. and Beck, K. A. (2004). A role for the spectrin superfamily member Syne-1 and kinesin II in cytokinesis. *J. Cell Sci.* **117**, 619-629.
- Gimona, M. and Winder, S. J. (1998). Single calponin homology domains are not actin-binding domains. *Curr. Biol.* **8**, 674-675.
- Gimona, M., Djinovic-Carugo, K., Kranewitter, W. J. and Winder, S. J. (2002). Functional plasticity of CH domains. *FEBS Lett.* **513**, 98-106.
- Goldman, R. D., Shumaker, D. K., Erdos, M. R., Eriksson, M., Goldman, A. E., Gordon, L. B., Gruenbaum, Y., Khuon, S., Mendez, M., Varga, R. et al. (2004). Accumulation of mutant lamin A causes progressive changes in nuclear architecture in Hutchinson-Gilford progeria syndrome. *Proc. Natl. Acad. Sci. USA* **101**, 8963-8968.
- Gomes, E. R., Jani, S. and Gundersen, G. G. (2005). Nuclear movement regulated by Cdc42, MRCK, myosin, and actin flow establishes MTOC polarization in migrating cells. *Cell* **121**, 451-463.
- Grady, R. M., Starr, D. A., Ackerman, G. L., Sanes, J. R. and Han, M. (2005). Syne proteins anchor muscle nuclei at the neuromuscular junction. *Proc. Natl. Acad. Sci. USA* **102**, 4359-4364.
- Gros-Louis, F., Dupre, N., Dion, P., Fox, M. A., Laurent, S., Verreault, S., Sanes, J. R., Bouchard, J. P. and Rouleau, G. A. (2007). Mutations in SYNE1 lead to a newly discovered form of autosomal recessive cerebellar ataxia. *Nat. Genet.* **39**, 80-85.
- Gruenbaum, Y., Margalit, A., Goldman, R. D., Shumaker, D. K. and Wilson, K. L. (2005). The nuclear lamina comes of age. *Nat. Rev. Mol. Cell Biol.* **6**, 21-31.
- Kandert, S., Lücke, Y., Kleinhenz, T., Neumann, S., Lu, W., Jaeger, V. M., Munck, M., Wehnert, M., Müller, C. R., Zhou, Z. et al. (2007). Nesprin-2 giant safeguards nuclear envelope architecture in LMNA S143F progeria cells. *Hum. Mol. Genet.* **16**, 2944-2959.
- Lechler, T. and Fuchs, E. (2005). Asymmetric cell divisions promote stratification and differentiation of mammalian skin. *Nature* **437**, 275-280.
- Libotte, T., Zaim, H., Abraham, S., Padmakumar, V. C., Schneider, M., Lu, W., Munck, M., Hutchison, C., Wehnert, M., Fahrenkrog, B. et al. (2005). Lamin A/C dependent localization of Nesprin-2, a giant scaffold at the nuclear envelope. *Mol. Biol. Cell* **16**, 3411-3424.
- Mislow, J. M., Holaska, J. M., Kim, M. S., Lee, K. K., Segura-Totten, M., Wilson, K. L. and McNally, E. M. (2002a). Nesprin-1alpha self-associates and binds directly to emerin and lamin A in vitro. *FEBS Lett.* **525**, 135-140.
- Mislow, J. M., Kim, M. S., Davis, D. B. and McNally, E. M. (2002b). Myne-1, a spectrin repeat transmembrane protein of the myocyte inner nuclear membrane, interacts with lamin A/C. *J. Cell Sci.* **115**, 61-70.
- Paddison, P. J., Caudy, A. A., Bernstein, E., Hannon, G. J. and Conklin, D. S. (2002). Short hairpin RNAs (shRNAs) induce sequence-specific silencing in mammalian cells. *Genes Dev.* **16**, 948-958.
- Padmakumar, V. C., Abraham, S., Braune, S., Noegel, A. A., Tunggal, B., Karakesisoglou, I. and Korenbaum, E. (2004). Enaptin, a giant actin-binding protein, is an element of the nuclear membrane and the actin cytoskeleton. *Exp. Cell Res.* **295**, 330-339.
- Padmakumar, V. C., Libotte, T., Lu, W., Zaim, H., Abraham, S., Noegel, A. A., Gotzmann, J., Foisner, R. and Karakesisoglou, I. (2005). The inner nuclear membrane protein Sun1 mediates the anchorage of Nesprin-2 to the nuclear envelope. *J. Cell Sci.* **118**, 3419-3430.
- Prufert, K., Vogel, A. and Krohne, G. (2004). The lamin CxxM motif promotes nuclear membrane growth. *J. Cell Sci.* **117**, 6105-6116.
- Schleicher, M., Gerisch, G. and Isenberg, G. (1984). New actin-binding proteins from *Dictyostelium discoideum*. *EMBO J.* **3**, 2095-2100.
- Starr, D. A. and Fischer, J. A. (2005). KASH 'n Karry: the KASH domain family of cargo-specific cytoskeletal adaptor proteins. *BioEssays* **27**, 1136-1146.
- Starr, D. A. and Han, M. (2002). Role of ANC-1 in tethering nuclei to the actin cytoskeleton. *Science* **298**, 406-409.
- Starr, D. A. and Han, M. (2003). ANChors away: an actin based mechanism of nuclear positioning. *J. Cell Sci.* **116**, 211-216.
- Tzur, Y. B., Wilson, K. L. and Gruenbaum, Y. (2006). SUN-domain proteins: 'Velcro' that links the nucleoskeleton to the cytoskeleton. *Nat. Rev. Mol. Cell Biol.* **7**, 782-788.
- Warren, D. T., Zhang, Q., Weissberg, P. L. and Shanahan, C. M. (2005). Nesprins: intracellular scaffolds that maintain cell architecture and coordinate cell function? *Expert Rev. Mol. Med.* **7**, 1-15.
- Wilhelmsen, K., Litjens, S. H., Kuikman, I., Tshimbalanga, N., Janssen, H., van den Bout, I., Raymond, K. and Sonnenberg, A. (2005). Nesprin-3, a novel nuclear membrane protein, associates with the cytoskeletal linker protein plectin. *J. Cell Biol.* **171**, 799-810.
- Winder, S. J., Hemmings, L., Maciver, S. K., Bolton, S. J., Tinsley, J. M., Davies, K. E., Critchley, D. R. and Kendrick-Jones, J. (1995). Utrophin actin binding domain: analysis of actin binding and cellular targeting. *J. Cell Sci.* **108**, 63-71.
- Yu, J., Starr, D. A., Wu, X., Parkhurst, S. M., Zhuang, Y., Xu, T., Xu, R. and Han, M. (2006). The KASH domain protein MSP-300 plays an essential role in nuclear anchoring during *Drosophila* oogenesis. *Dev. Biol.* **289**, 336-345.
- Yuspa, S. H., Hawley-Nelson, P., Koehler, B. and Stanley, J. R. (1980). A survey of transformation markers in differentiating epidermal cell lines in culture. *Cancer Res.* **40**, 4694-4703.
- Zhang, Q., Ragnauth, C. D., Skepper, J. N., Worth, N. F., Warren, D. T., Roberts, R. G., Weissberg, P. L., Ellis, J. A. and Shanahan, C. M. (2005). Nesprin-2 is a multi-isoform protein that binds lamin and emerin at the nuclear envelope and forms a subcellular network in skeletal muscle. *J. Cell Sci.* **118**, 673-687.
- Zhang, Q., Bethmann, C., Worth, N. F., Davies, J. D., Wasner, C., Feuer, A., Ragnauth, C. D., Yi, Q., Mellad, J. A., Warren, D. T. et al. (2007). Nesprin-1 and -2 are involved in the pathogenesis of Emery Dreifuss muscular dystrophy and are critical for nuclear envelope integrity. *Hum. Mol. Genet.* **16**, 2816-2833.
- Zhang, X., Xu, R., Zhu, B., Yang, X., Ding, X., Duan, S., Xu, T., Zhuang, Y. and Han, M. (2007). Syne proteins anchor muscle nuclei at the neuromuscular junction. *Development* **134**, 901-908.
- Zhen, Y. Y., Libotte, T., Munck, M., Noegel, A. A. and Korenbaum, E. (2002). NUANCE, a giant protein connecting the nucleus and actin cytoskeleton. *J. Cell Sci.* **115**, 3207-3222.